

Stability Analysis of Bridged Cracks in Brittle Matrix Composites

R. Ballarini
Associate Professor.

S. Muju
Graduate Student.

Department of Civil Engineering,
Case Western Reserve University,
Cleveland, OH 44106

The bridging of matrix cracks by fibers is an important toughening mechanism in fiber-reinforced brittle matrix composites. This paper presents the results of a non-linear finite element analysis of the Mode I propagation of a bridged matrix crack in a finite size specimen. The composite is modeled as an orthotropic continuum and the bridging due to the fibers is modeled as a distribution of tractions that resist crack opening. A critical stress intensity factor criterion is employed for matrix crack propagation, while a critical crack opening condition is used for fiber failure. The structural response of the specimen (load-deflection curves) as well as the stress intensity factor of the propagating crack is calculated for various constituent properties and specimen configurations for both tensile and bending loading. By controlling the length of the bridged crack, results are obtained that highlight the transition from stable to unstable behavior of the propagating crack.

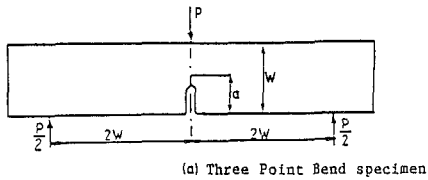
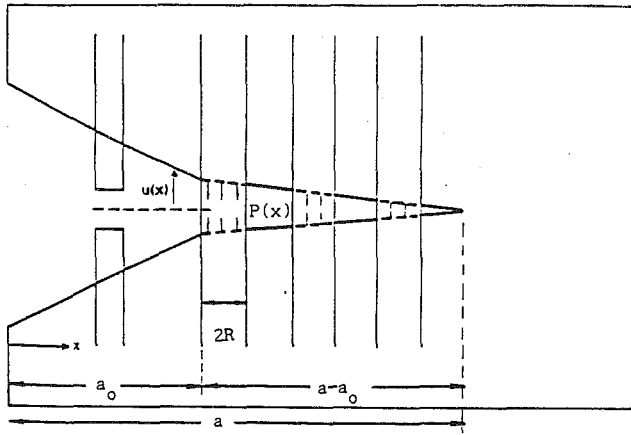
Introduction

Crack bridging is an important toughening mechanism in many engineering materials, including fiber and whisker-reinforced ceramic and metal matrix composites, plain and fiber-reinforced concrete, matrices reinforced with ductile secondary phases, and glassy polymers. This fact has led to a significant amount of research aimed at gaining a better understanding of the mechanics of bridged cracks. Various models have been proposed by researchers in different fields in which the bridging is modeled as a distribution of discrete forces or continuous stresses which resist crack opening. While they differ in the conditions specified to calculate the lengths of the bridging zone and the propagation criterion, all of the proposed models are essentially of the Dugdale-Barenblatt type [1, 2].

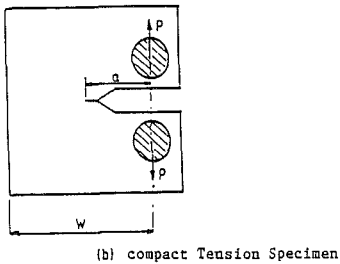
A typical model for a bridged crack is shown in Fig. 1(a). The "effective" crack length is the sum of a traction-free length and of a "process zone," within which a traction is prescribed that models the bridging arising from the active mechanisms. In this figure the process zone consists of fibers. However, the mechanisms may include aggregate interlock, microcracking, crazing, plastic yielding, fiber bridging, etc. In metals the Dugdale model has been used to simulate yielding ahead of a crack tip. In this model the closing stress is equal to the yield stress of the material, and the length of the process zone is calculated by requiring the stress intensity factor due to the closing stress to cancel the one resulting from the applied loading. Propagation is assumed to occur when the crack opening displacement at the tip of the traction-free crack reaches a specified critical value. The reason the stress intensity factor is taken as zero is that the energy release rate associated with the stress

intensity factor is negligible compared to the energy dissipated in the yielding process. A zero net stress intensity factor has also been assumed in several models for plain and fiber-reinforced mortar and concrete [3, 4], since the energy dissipated in the stretching of steel fibers is much greater than the fracture energy of the matrix. In these strain-softening materials the closing stress is taken as a monotonically decreasing function of crack opening displacement [3-6]. In composites composed of brittle fibers and matrix, the assumption that the fracture toughness of the matrix is negligible is not valid. Marshall and Cox [7, 8] have developed a model for ceramic matrix composites in which the crack is assumed to propagate when the net stress intensity factor reaches the critical stress intensity factor of the matrix. Using a micromechanical model they determined [7] that the stress that resists crack opening is proportional to the square root of the crack opening displacement. Using this relation, they obtained extensive numerical results, which provide a much better understanding of possible failure mechanisms in tension loaded ceramic matrix composites. In particular, they showed that the fiber strength is a parameter that governs whether a matrix crack will be fully bridged or partially bridged as it propagates through the specimen. Strong fibers lead to fully bridged cracks, which can grow in the matrix through the specimen while the fibers remain intact. As shown schematically in Fig. 2, this "noncatastrophic," or "ductile" mode of failure leads to large strains, since further loading beyond the first matrix crack leads to multiple matrix cracking and an ultimate strength, which is governed by the bundle strength. Relatively weak fibers, on the other hand, lead to matrix cracks, which are bridged in a relatively small region behind the crack tip as they propagate. Moreover, as a partially bridged crack propagates, the fibers behind the crack tip break sequentially, eventually breaking the specimen in two. In this paper a model similar to the one

Contributed by the International Gas Turbine Institute and presented at the 36th International Gas Turbine and Aeroengine Congress and Exposition, Orlando, Florida, June 3-6, 1991. Manuscript received at ASME Headquarters February 19, 1991. Paper No. 91-GT-94. Associate Technical Editor: L. A. Rieker.



(a) Three Point Bend specimen



(b) compact Tension Specimen

Fig. 1 Crack configuration and typical fracture specimens

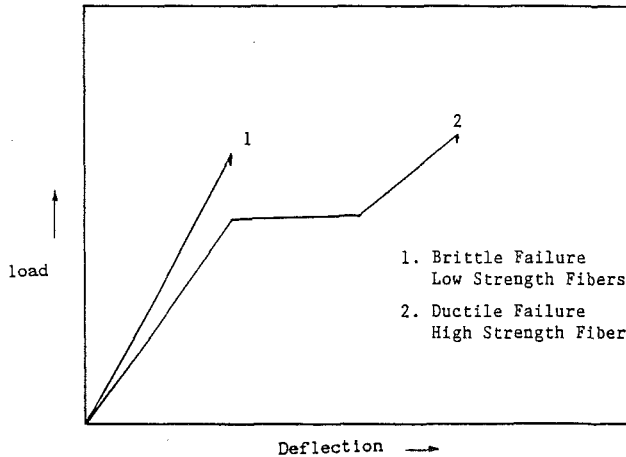


Fig. 2 Possible failure modes of brittle matrix composites

developed by Marshall and Cox is used to study the effects of loading and specimen size on the behavior of bridged cracks in continuously reinforced brittle matrix composites. Of particular interest in this study is the transition from ductile to brittle behavior of such cracks, and how this transition is affected by constituent properties, specimen size, and type of loading. This transition will be highlighted by controlling the length of the bridged crack, as was done by Carpinteri [9] in his study of crack growth in concrete. In the course of this investigation the authors became aware that Cox and Marshall [10, 11], using an integral equation approach, performed an

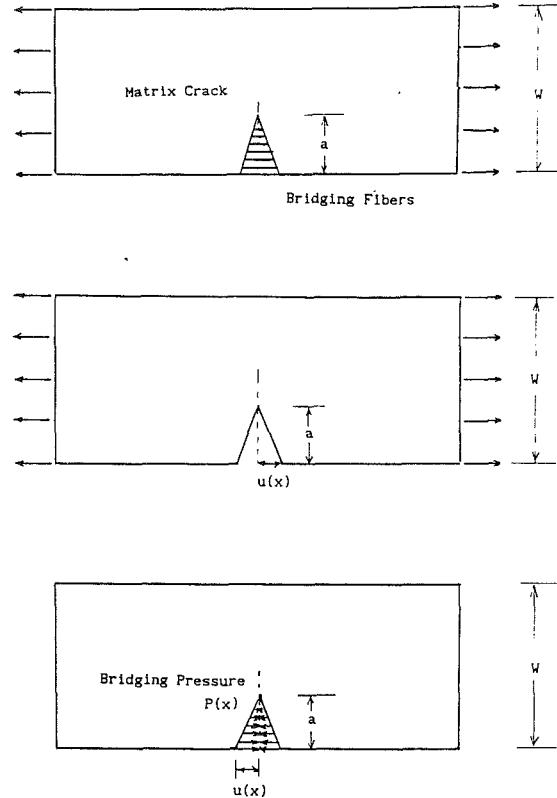


Fig. 3 Superposition scheme

analysis similar to the one presented in this paper. The advantage of the numerical model presented in this paper is its ability to treat complicated geometries, anisotropic materials, nonhomogeneous structures, and cracks that propagate in directions that do not coincide with principal axes.

Finite Element Model

The present work is directed toward developing a numerical analysis tool that can be used to analyze anisotropic fracture specimens of finite size. Typical examples include, as shown in Fig. 1(b), the edge-notched beam and the compact tension specimens. Moreover, the crack surfaces are bridged as shown in Fig. 1(a). The fibers within a distance $a - a_0$ from the crack tip remain intact and bridge the crack, while the remaining fibers over distance a_0 from the crack mouth are broken and do not contribute to crack tip shielding. Failure of the composite may be initiated either by fiber failure or matrix crack growth.

The influence of fiber shielding is to restrain the crack opening, and, consequently, reduce the stress field in the vicinity of the matrix crack tip. The bridged crack can be viewed as the superposition of a traction-free crack subjected to a remote loading, and a crack whose surfaces are loaded with the forces arising from the fibers (Fig. 3). For closely spaced fibers and relatively long cracks, the discrete forces are assumed to be equivalent to a continuous distribution of closing stress $p(x)$. This superposition can be performed using different techniques. For cracks in infinite bodies and for relatively simple finite geometries, a singular integral equation approach can be used. With this approach the problem is reduced to an integral equation, which represents the traction boundary condition along the crack surfaces. The integral equation is then solved for the unknown dislocation density along the crack line, which can be used to calculate relevant physical quantities such as stress intensity factor and crack opening displacement. Because the closing stress is a nonlinear function of the crack

opening displacement, or dislocation density, the integral equation is nonlinear and an iterative solution is needed. This approach has been used in studies of plain and fiber reinforced concrete [6]. An integral equation approach in which the crack opening displacements are treated as unknowns has been used for ceramic matrix composites [7, 8, 10, 11].

In the present work, the finite element method is implemented for this superposition. The physics is assumed as follows. The matrix crack will propagate when the stress intensity factor in the matrix reaches a critical value K_{IC}^m , which is related to the composite stress intensity, K_{IC}^c , by the relation $K_{IC}^c = K_{IC}^m E_c / E_m$ [7]. This relation is based on strain compatibility between fibers and matrix, and hence is not rigorously valid for very short cracks, nor for fibers slipping ahead of the crack tip. The closing stress relation is given by [7]

$$p(x) = 2V_f[\tau E_f(1 + \eta)/R]^{1/2}(u(x))^{1/2} \quad (1)$$

where

$V_f(V_m)$ = volume fraction of fibers (matrix)

τ = interfacial shear strength

$E_f(E_m)$ = elastic modulus of fiber (matrix)

R = fiber radius

$\eta = E_f V_f / E_m V_m$

$u(x)$ = crack opening displacement

Equation (1), which represents a closing stress that increases monotonically with crack opening displacement, was derived with the assumption of a single valued fiber strength. A closing stress function that initially increases and subsequently decreases was derived, assuming the fiber strengths satisfy weakest link theory, by Thouless and Evans [12]. Their analysis led to the following equation for the stress displacement relation for the bridging fibers:

$$(\sigma/\Sigma) = (u/u_n)^{1/2} \exp[-(u/u_n)^{(m+1)/2}] + \frac{1}{(1+\eta)(m+1)} \{1 - \exp[-(u/u_n)^{(m+1)/2}]\} \times \left\{ \gamma[(m+2)/(m+1), (u/u_n)^{(m+2)/2}] - \frac{\Sigma(m+1)}{2E_f} \left[\frac{u}{u_n} \right] \right\} \quad (2)$$

where

$$\Sigma = \langle s \rangle / \Gamma \left[\frac{m+2}{m+1} \right]$$

$$u_n = \frac{\Sigma^2 R (1 - V_f) E_m}{4\tau E_f E}$$

m = Weibull modulus of fiber strength distribution

$\langle s \rangle$ = Average strength of the fiber bundle

$$\gamma[(m+2)/(m+1), \alpha] = c \int_0^\alpha \beta^{1/(m+1)} e^{-\beta} d\beta$$

$$\Gamma(\delta) = \int_0^\infty \beta^{\delta-1} \exp(-\beta) d\beta$$

$$\alpha = (u/u_n)^{(m+1)/2}$$

For the case of single-valued strength fibers, $m = \infty$, $\langle s \rangle = \sigma_{fu}$, where σ_{fu} is the ultimate fiber strength, and Eq. (2) reduces to Eq. (1), which is used in the present analysis. A recent analysis of tension loaded notched beams by Cox and Marshall [11] was performed for several values of m . Equation (1) can be conveniently represented as

$$p(x) = \begin{cases} A\sqrt{u(x)} & x \geq a_o \\ 0 & x \leq a_o \end{cases} \quad (3a)$$

where

$$A = 2V_f[E_f\tau(1 + \eta)/R]^{1/2} \quad (3b)$$

The quantity u_n corresponds to the critical opening, which

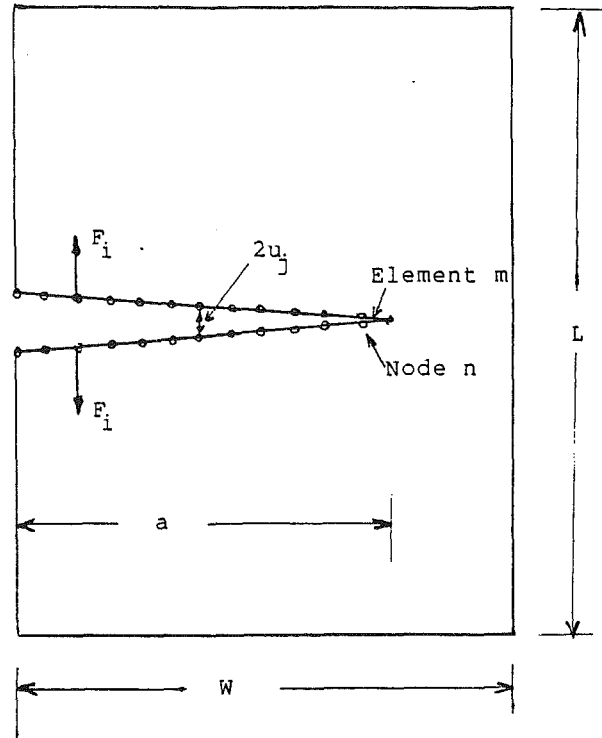


Fig. 4 Finite element nodes representing the crack line

produces a stress in the fiber equal to σ_{fu} . In this work fiber failure is assumed to occur when the crack opening equals u_n . It should be noted that the assumption of single-valued strength implies that fiber failure first occurs at the far edge of the bridging zone, since the crack opening displacements decrease monotonically towards the crack tip (this has been confirmed in [8] and in the present work). A statistical fiber strength distribution may lead to fibers nearest to the crack mouth remaining intact while others closer to the crack tip breaking.

With reference to Fig. 4, n nodes are distributed along the fracture line. The crack opening displacements can be represented as

$$u_i = K_{ij}F_j + \sigma C_i \quad i, j = 1, \dots, n \quad (4)$$

where

u_i = crack opening at node i

F_j = load (due to the fibers) at node j

C_i = influence coefficients representing crack opening at node i due to unit applied far field stress

K_{ij} = influence coefficients representing crack opening at node i due to unit load F_j

σ = applied stress

The load point deflection can be represented as

$$\Delta = D_j F_j + \sigma \Delta_o \quad j = 1, \dots, n \quad (5)$$

where

D_j = influence coefficients for load-point displacement due to F_j

Δ_o = load-point displacement due to unit applied stress.

Equations (4) and (5) can be modified for any far-field loading by appropriately modifying the remote loading σ . For the single-edge notch specimen considered in this paper, the deflection Δ is measured, for tensile loading, at point A of the typical finite element model shown in Fig. 5, while for the three-point bend loading, it is measured at the point B. The specimen has length $L = 20$ cm and width $W = 5$ cm. The geometry is modeled with quadratic elements. To calculate the

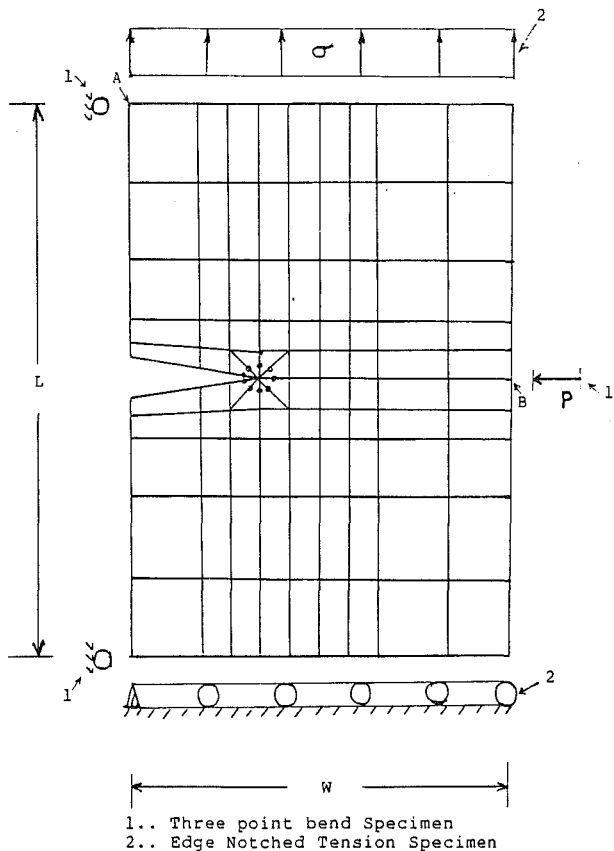


Fig. 5 Schematic of finite element model for constant tension and three-point bending

stress intensity factors accurately, the elements emanating from the crack tip were converted to singularity elements by shifting their midside nodes to the quarter point. The stress intensity factor calibration, which provides the Mode I and Mode II stress intensity factors as functions of the displacements of certain nodes of the singularity elements behind the crack tip, is given in [13]. The K_{ij} and C_i were calculated for the orthotropic material by modifying the element stiffness matrix of an isotropic finite element program. Although the comparisons are not presented here, the stress intensity factors calculated for $p(x)=0$ agreed within a few percent with those presented by Bowie [14] for the tested values $0.1 \leq a/w \leq 0.7$.

The system was loaded in $n+1$ different loading conditions, corresponding to unit loads at each node and a unit far field stress. For each loading case the displacements of each node were calculated including the load-point displacement. This procedure provided the $n \times n$ terms of K_{ij} , and the n terms of C_i . Note that the global stiffness matrix needs to be inverted only once for a given crack length. Once the coefficients are calculated, the problem is reduced to a system of n nonlinear algebraic equations as follows. Recalling that $p(x) = A\sqrt{u(x)}$, the expression for nodal forces becomes

$$F_j = A \frac{a}{2q} \sqrt{u_j} = \bar{A} (u_j)^{1/2} \quad (6)$$

where a is the crack length and q is the number of quadratic displacement elements along the crack line. The resulting system of equations for crack opening becomes

$$u_i = \bar{A} [K_{ij}] u_j^{1/2} + \sigma [C_i] \quad i, j = 1, \dots, n \quad (7)$$

The nonlinear system of equations was solved using the IMSL routine 'DNEQNF,' which is based on the Levenberg-Marquadt and Powell algorithms [15].

It should be noted that Eq. (6) assumes that each node acts as an independent (leaf) spring. Although the work-equivalent

Table 1 Constitutive material properties

Constituent	Young's modulus, GPa	Poisson ratio	K_{IC} MPa \sqrt{m}
SiC fibers	390	0.3	5.0
Si ₃ N ₄ matrix	206	0.3	4.6

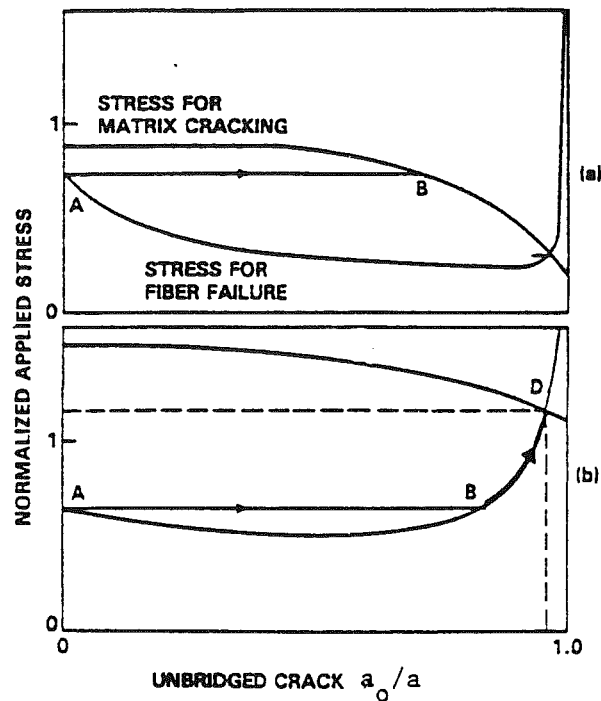


Fig. 6 Possible failure modes for brittle matrix composites [8]

nodal forces for the distributed closing stress for a quadratic element should be used in the calculations, numerical experimentation showed differences of approximately 4 percent in stress intensity factors between "exact" nodal forces and the "leaf" springs. Subsequent results were calculated using independent springs.

Results

The material properties used for the constituents are shown in Table 1. They correspond to the properties of a SiC reinforced Si₃N₄ matrix composite. The volume fraction of the 100 μm -dia ($2R$ in Fig. 1a) fibers is $V_f=0.4$. The shear strength of the fiber-matrix interface is taken as $\tau=10$ MPa. Consistent with these values, the orthotropic bulk properties are [16, 17]: $E_{11}=253.9$ GPa, $E_{22}=279.6$ GPa, $\nu_{12}=0.3$, and $G_{12}=97.66$ GPa.

Composite failure is initiated when the applied stress exceeds the smaller of the matrix cracking stress σ_m (the stress that makes the stress intensity factor in the matrix equal to the fracture toughness of the matrix) and fiber failure stress σ_f . Subsequent failure events (at constant applied stress) involve combinations of stable and unstable fiber failure and/or matrix cracking. The sequence of these events depends on initial crack configuration a and a_0 , specimen configuration, type of loading, and fiber strength σ_{fu} . As shown in Fig. 6, taken from [8], for initially fully bridged cracks two different sequences of failure events are possible for the case when the fiber failure stress is less than the matrix cracking stress. The first corresponds to the case in which the matrix cracking stress is slightly greater than the first fiber failure stress. Fiber failure initiates at point A and is unstable until point B. At this point the matrix cracks. Beyond point B the fibers fail as the matrix crack propagates. The second possibility corresponds to a ma-

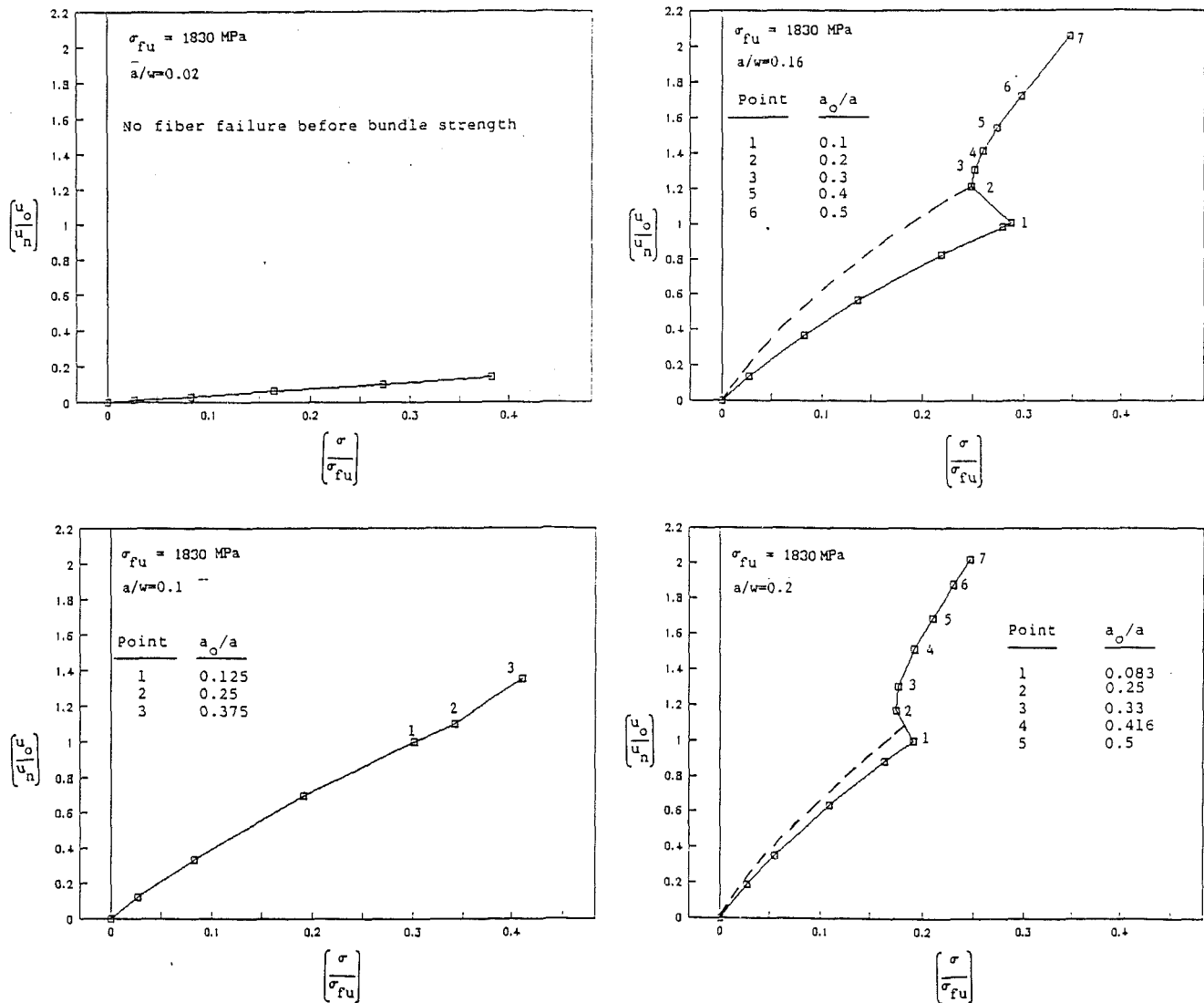


Fig. 7 Normalized CMOD as functions of normalized applied stress, tensile loading

trix cracking stress much greater than the fiber failure stress. In this case fiber failure is initiated at point *A* and is unstable until point *B*. At point *B* the system stabilizes. That is, an increasing stress is required to break additional fibers. This continues until point *D*, at which point the matrix cracks in an unstable manner. The third possible scenario corresponds to high fiber strengths in which the matrix cracks without any fiber failure, and hence the matrix cracks through the specimen leaving fibers intact. All of these possible events have been captured in the present analysis by varying σ_{fu} and crack length.

Two types of simulation were performed in this work for each type of loading (tension and bending). In the first, the total crack length was held constant while the load was monitored in such a way as to capture the stability characteristics of fiber failure. In these simulations the stress intensity factor at the tip of the matrix crack was not specified. The second type corresponds to a matrix crack propagating at a constant specified value of stress intensity factor. All of the cracks considered are initially fully bridged.

Fixed Crack Length Simulations—Constant Stress Loading

Effects of a/w . Numerical calculations were performed first for tension loading at fixed crack lengths in the range

$0.02 \leq a/w \leq 0.8$. However, only the results for $0.02 \leq a/w \leq 0.2$ are presented, since it was observed that for the tension loading and the considered specimen width the stable to unstable transition occurs in this range.

In the first type of simulation the far-field stress is increased for a fixed length, initially fully bridged crack until the crack opening at a point reaches the critical value u_n . When this critical crack opening is reached at a node, the node is released, and the applied stress is either increased or decreased, depending on the stability of fiber failure. If the stress level has to be increased to break additional fibers, the event is termed stable. If the stress level that produces fiber failure at a node is held constant, and additional fibers fail, the event is termed unstable. It may be possible, however, for unstable events to stabilize. For the unstable events, the load has to be controlled in order to capture the sequence of fiber failure (trace the unstable path).

Figures 7(a-d) are plots of normalized crack mouth opening displacement (CMOD) u_o as functions of normalized stress for $\sigma_{fu} = 1830$ Mpa. For very short crack lengths ($a/w = 0.02$) no fiber failure occurs for normalized stress levels less than 0.4, which corresponds to the bundle strength $V_f \sigma_{fu}$. This implies that most likely matrix cracking will occur before any fiber failure. For $a/w = 0.1$ the failure of the first fiber is stable, since increasing stress is required for additional fiber failure.

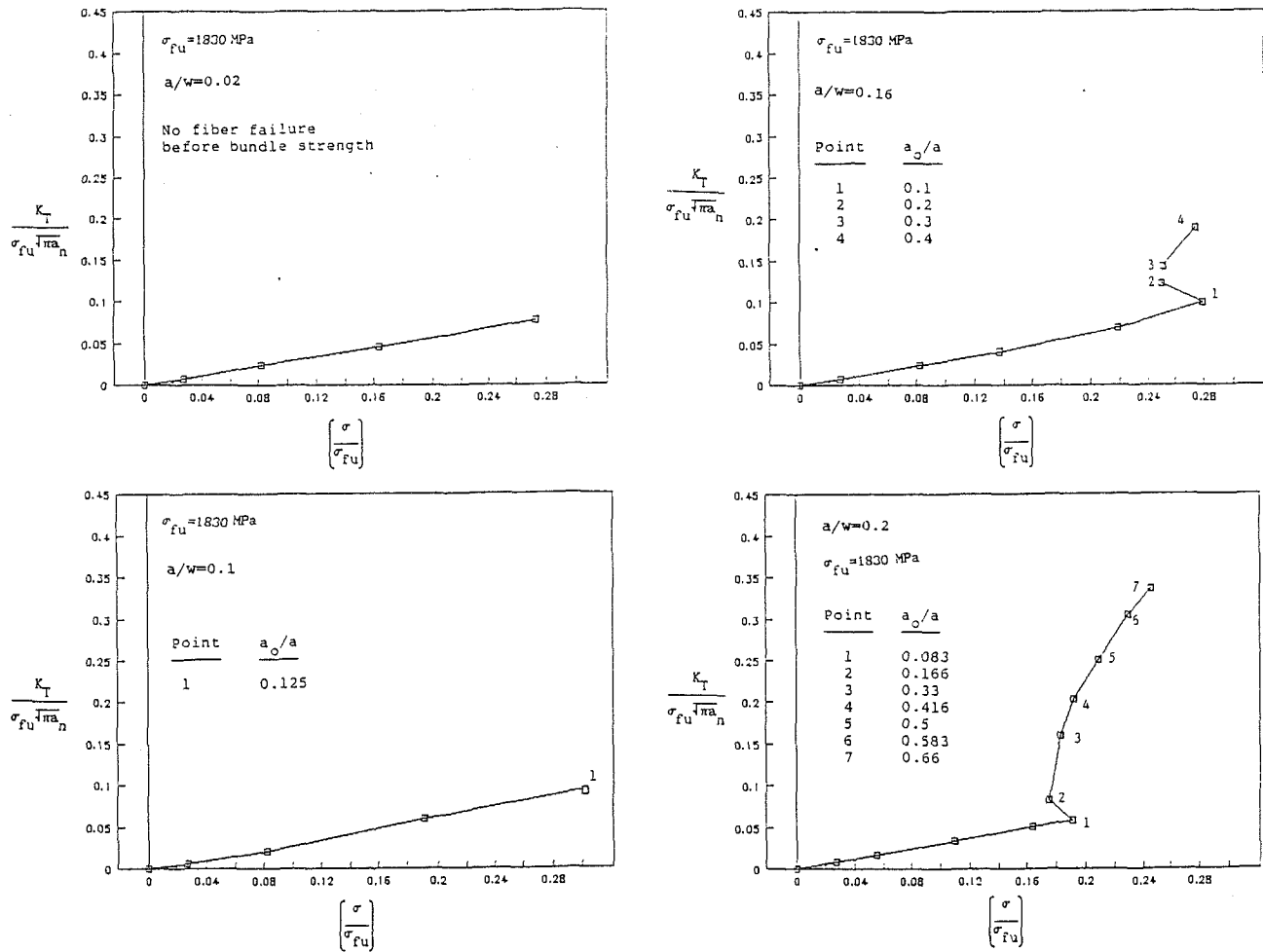


Fig. 8 Normalized stress intensity factor as functions of applied stress, tensile loading

For cracks longer than $a/w=0.16$, initial fiber failure (until $a_o/a=0.1$) is unstable. Fiber failure stabilizes, for this configuration, at $a_o/a \cong 0.4$. Consider point 1 in Fig. 7(c). If the stress were held constant, additional fibers would fail until $a_o/a \cong 0.4$. The stress would then have to be increased to break additional fibers. Moreover, if the stress is not decreased at point 1, subsequent fiber failure produces a discontinuity in the CMOD.

Consider next the stress intensity factors. The net stress intensity factor K_T is related to the far-field (K_A) and fiber bridging (K_F) stress intensity factors by $K_T = K_A - K_F$, so that the shielding due to the fibers is $K_F = K_A - K_T$.

Figures 8(a-d) and 9(a-d) are plots of normalized K_T and K_F , respectively, as functions of applied stress. The length a_n is defined by

$$a_n = [\pi \Sigma R (1 - V_f) E_m] / [16 \tau V_f E_f (1 - \nu^2)] \quad (8)$$

As discussed in [11], a_n , which is associated with a fully bridged crack in an infinitely extended material and is referred to as the bridging length scale, has special significance. For $a < a_n$, the crack is considered short in the sense that its bridging zone is still developing. For these short fully bridged cracks the forces in the fibers are relatively small, since the crack opening displacements are small. Hence the fibers do not shield the crack tip significantly, and the stress required to propagate the matrix crack is inversely proportional to the square root of the crack length, as for a monolithic matrix. For $a > a_n$ the crack is termed long, because the bridging zone has fully developed and a steady state is reached for matrix cracking (the

stress required to propagate the matrix crack is independent of crack length). For the considered composite $a_n = 0.256$ mm, 1.56 mm, and 2.56 mm for fiber strengths (which will be discussed subsequently) $\sigma = 300$ MPa, 1830 MPa, and 3000 MPa, respectively.

The stability of the fiber failure can also be seen in these figures. For example, compare K_F for $a/w=0.02$ and $a/w=0.16$. For 0.02 the shielding monotonically increases, while for 0.16 there is a sharp reduction after the first nodal failure (which corresponds to the discontinuous increase in K_T in Fig. 8c). Also note that for 0.16, even if the stress is reduced at the point of first fiber failure, the net stress intensity factor still increases. If the normalized matrix toughness were high enough (above point 4 in Figs. 8c and 8d), unstable nodal failure would occur before matrix cracking until $a_o/a \cong 0.4$, at which point the fiber failure stabilizes. If, on the other hand, the matrix toughness is below point 1, the matrix would crack before fiber failure.

From these graphs the qualitative response of initially partially bridged cracks can also be seen. Take, for example, Fig. 7(c). If a partially bridged crack of total length $a/w=0.16$ ($a_o/a=0.2$) has propagated in the matrix from an initial (unbridged) notch of length a/w ($a_o/a=1.0$), no instability would be observed, since the CMOD versus applied stress curve would be as shown in dashed lines. For a crack length $a/w=0.2$ with the same unbridged length ($a_o/a=0.16$), the curve would be also as shown in dashed lines, and instability would still be observed. This suggests that for initially partially bridged cracks the transition from stable to unstable fiber failure occurs at longer crack lengths.

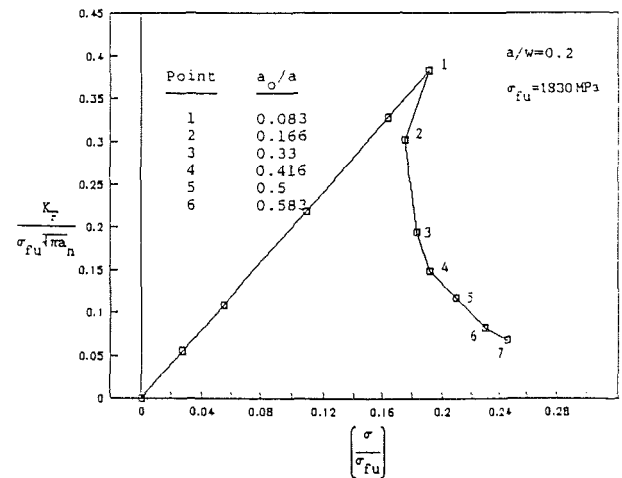
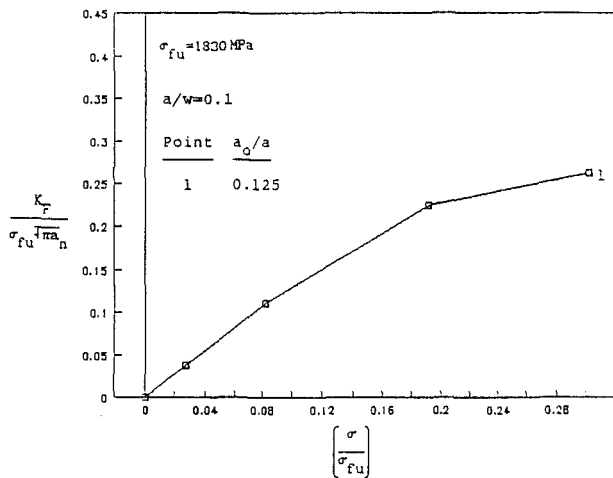
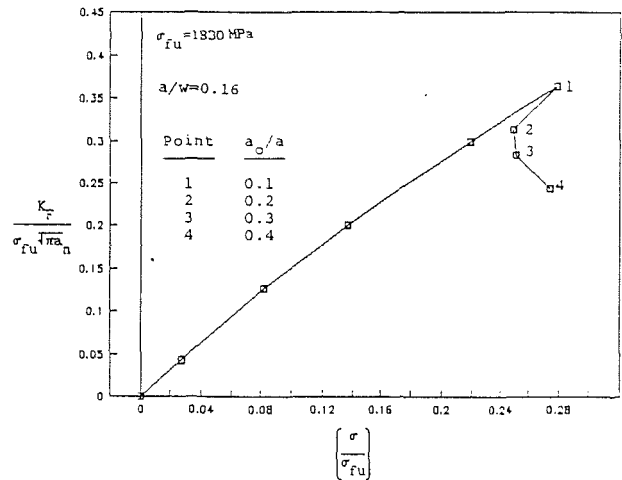
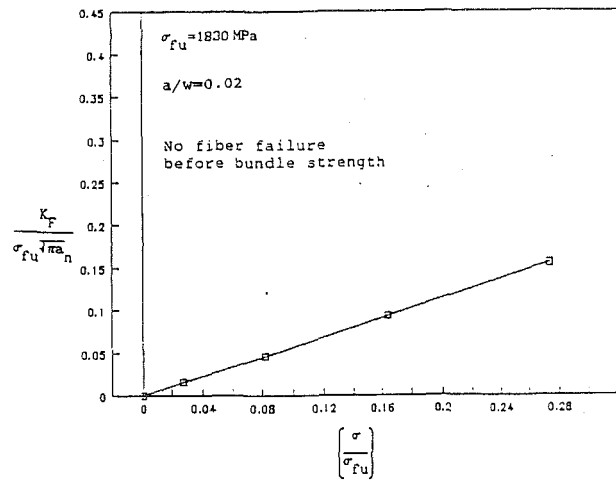


Fig. 9 Normalized shielding stress intensity factor as functions of applied stress, tensile loading

Effects of σ_{fu} . To investigate the effects of fiber strength on the stability of fiber failure, the following values of fiber strength were used: $\sigma_{fu} = 300, 1830,$ and 3000 MPa .

The effects of fiber strength on the stability of fiber failure can be observed by comparing Figs. 7(d) and 10(a). For $\sigma_{fu} = 1830 \text{ MPa}$, initial fiber failure is unstable, but stabilizes at $a_o/a \cong 0.42$. For $\sigma_{fu} = 3000 \text{ MPa}$, on the other hand, unstable fiber failure does not stabilize.

This effect can also be observed by comparing Figs. 8(d) and 10(b). The net stress intensity factor for the lower fiber strength increases monotonically as the unstable fiber failure is traced. However, an increasing stress is needed to increase the net stress intensity factor after fiber failure stabilizes. For the higher fiber strength, on the other hand, as the unstable path is traced, the stress intensity factor increases drastically at stress levels less than the level that caused first fiber failure. These differences are also observed in Figs. 9(d) and 10(c), which show that the reduction in shielding beyond first fiber failure for the higher fiber strength is much more drastic than for the lower strength.

Matrix Crack Propagation Simulations—Constant Stress Loading

In these simulations, an initially fully bridged crack of length $a/w = 0.02$ is loaded until the stress intensity factor at its crack tip is equal to the fracture toughness of the matrix, taken as $4.6 \text{ MPa}\cdot\text{m}^{1/2}$. As the load is increased, if the crack opening displacement at any node reaches u , the node is released. When

the stress intensity factor reaches the critical value, the matrix crack is extended.

Load Deflection Curves. Figure 11(a) is a plot of applied stress versus load point displacement for $\sigma_{fu} = 300 \text{ MPa}$. Figure 11(b) is an enlarged view of the snap back region in Fig. 11(a). The stress is increased until point 1, at which time approximately 63 percent of the fibers behind the crack tip have failed, and the matrix cracks. The matrix crack extends to $a/w = 0.1$. At this point the stress is reduced to point 2, at which time the fibers at the trailing edge of the bridging zone start breaking. The stress is then increased until point 7, at which time all the nodes are released (it may be possible that a few fibers remain intact, but since the first node behind the crack tip is a finite distance from the crack tip, this is not captured), $a_o/a = 1.0$, and the matrix crack extends to $a/w = 0.2$, with $a_o/a = 1.0$. This process of complete fiber rupture/matrix crack extension continues (points 10, 12, 14) until point 16 at which point $a/w = 0.6$. Figure 11(a) was obtained by monitoring the fiber failure events. If the total crack length were controlled the stress-deflection curve would be as shown in Fig. 12. Note, however, that information is gained by monitoring the fiber failure events. For example, if the stress is kept constant at point 1 of Fig. 11(a) (or point A of Fig. 12), the extension of the matrix crack through the specimen is accompanied by simultaneous fiber failure. Thus the failure is catastrophic.

For $\sigma_{fu} = 1830 \text{ MPa}$, Figs. 13 and 14 show that the failure is not catastrophic, since as the matrix crack propagates through the specimen most of the fibers behind the crack remain intact ($a_o/w \cong 0.25$). Although the simulations were not continued

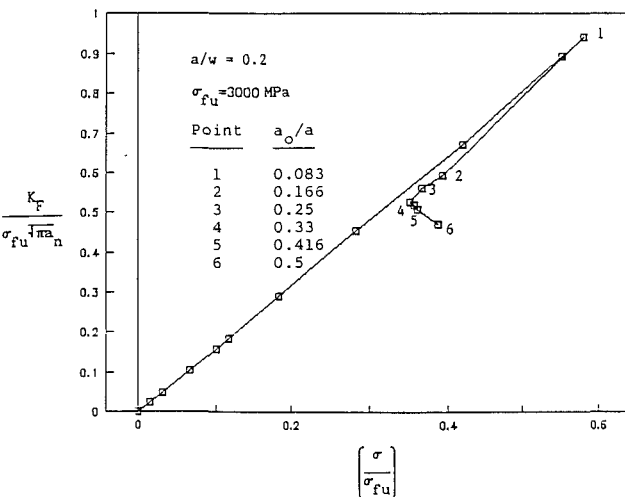
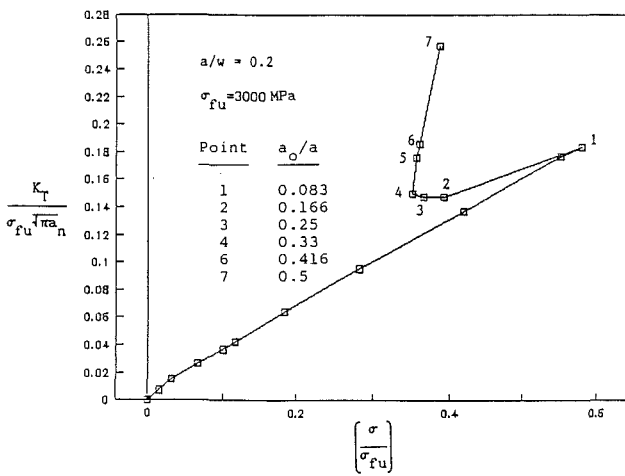
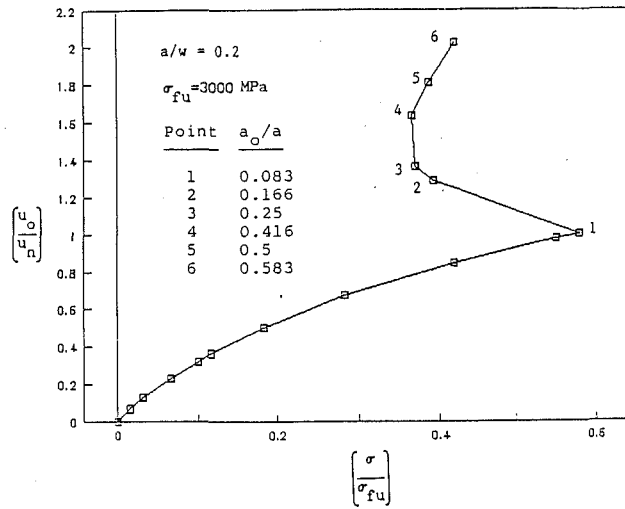


Fig. 10 Normalized (a) CMODs, (b) stress intensity factors, and (c) shielding stress normalized applied stress, tensile loading

beyond point 16 in Fig. 13, an increase in stress is needed to break the remaining fibers.

For the highest fiber strength considered, Fig. 15 shows that the matrix crack propagates through the specimen while all the fibers behind the crack tip remain intact. This will lead to

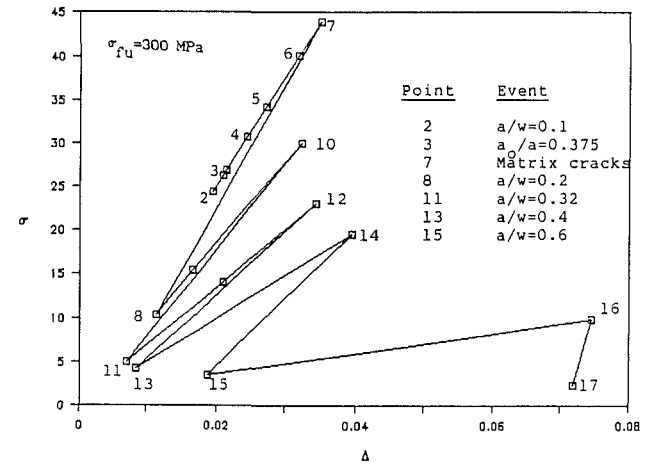
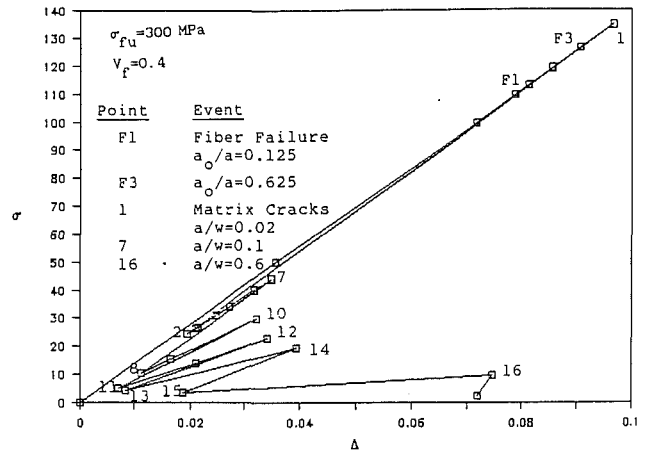


Fig. 11 Stress-deflection curves, tensile loading

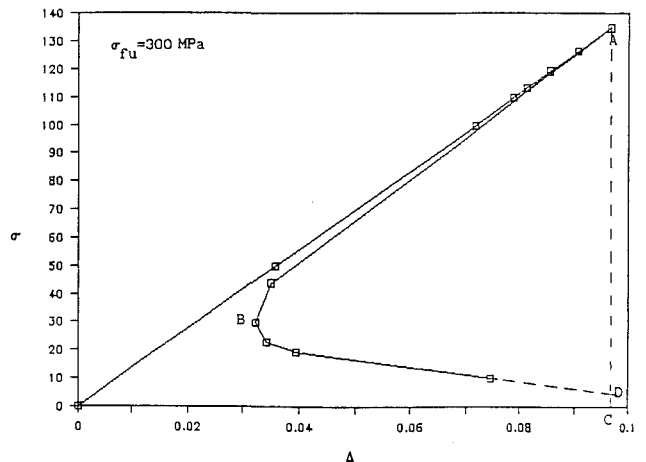


Fig. 12 Stress-deflection curve, tensile loading

multiple matrix cracking and an ultimate strength governed by the bundle strength.

The stress-deflection curves clearly demonstrate the brittle to ductile transition of the considered initially fully bridged cracks. It should also be noted that the critical stress for crack extension and the strain to failure are higher for the noncatastrophic failure modes than for the catastrophic failure modes.

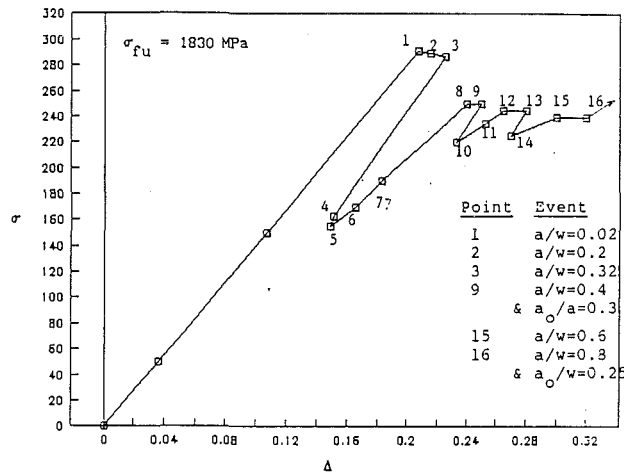


Fig. 13 Stress-deflection curve, tensile loading

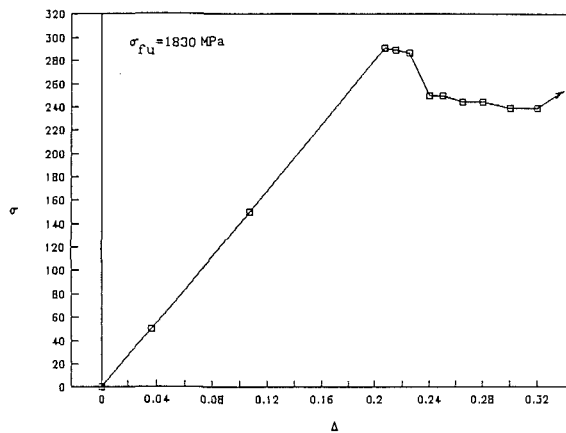
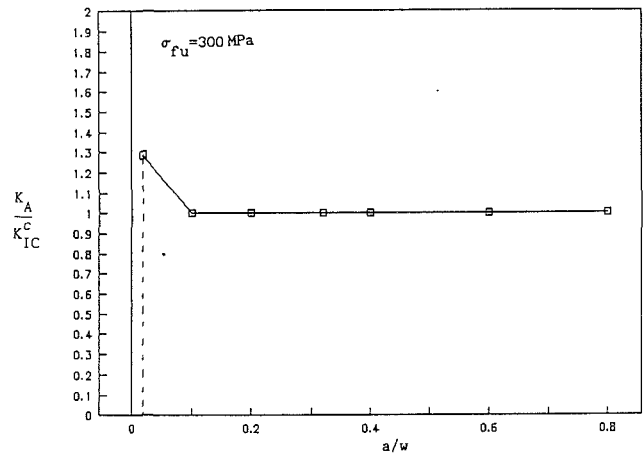


Fig. 14 Stress-deflection curve, tensile loading

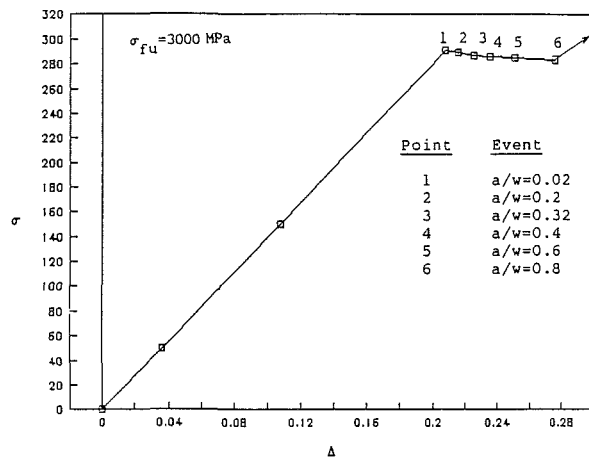
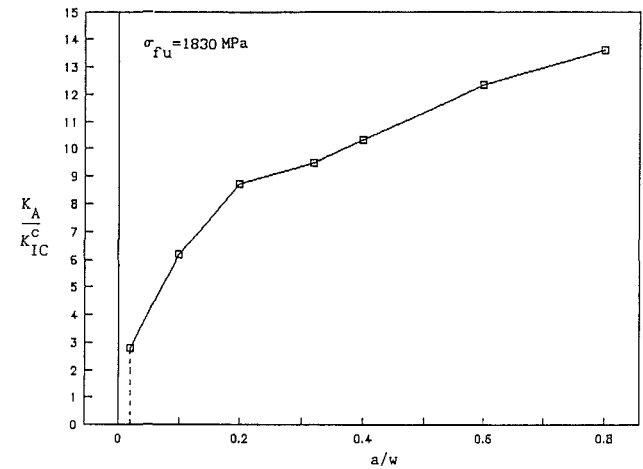


Fig. 15 Stress-deflection curve, tensile loading

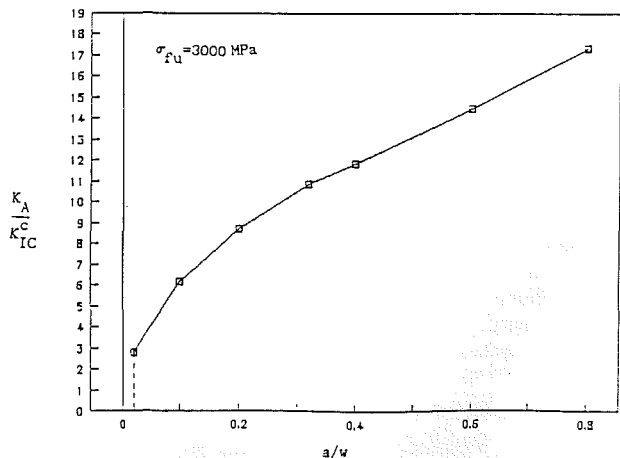


Fig. 16 Normalized resistance curves, tensile loading

Resistance Curves. Figures 16(a-b) are plots of the normalized applied stress intensity factor, which leads to matrix crack growth as functions of matrix crack length for the different fiber strengths. For $\sigma_{fu} = 300$ MPa, the applied stress intensity factor is greater than the fracture toughness of the matrix for $a/w \leq 0.1$, since the crack is partially bridged. Beyond $a/w = 0.1$ the normalized applied stress intensity factor

is equal to 1.0, since for each crack length all the fibers break before the matrix crack extends.

For $\sigma_{fu} = 1830$ MPa, Fig. 16(b) shows that the applied stress intensity factor increases monotonically as the matrix crack extends through the specimen. For this value of fiber strength

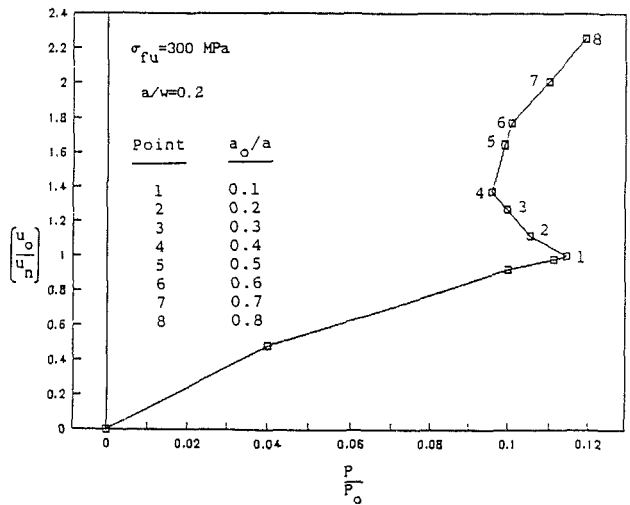
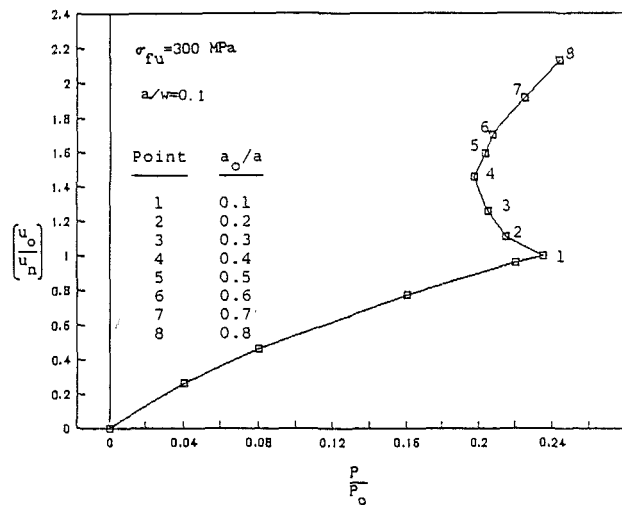
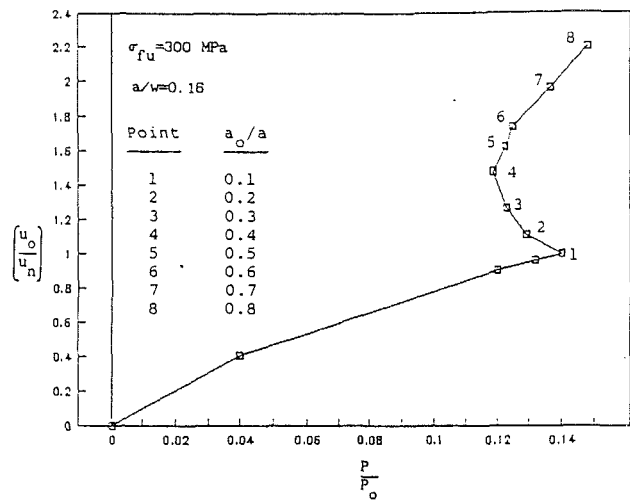
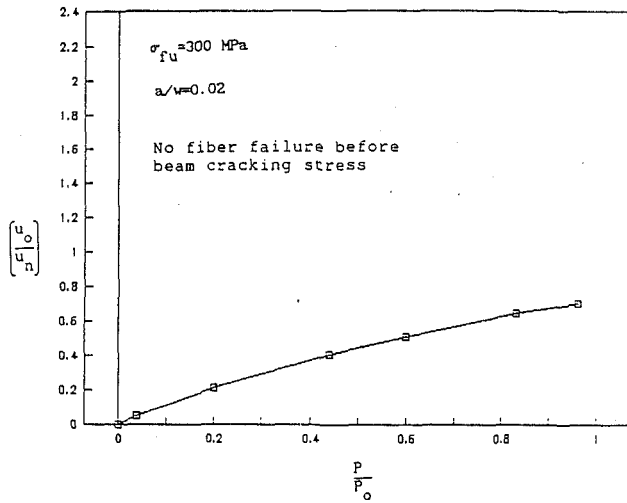


Fig. 17 Normalized CMOD as functions of three-point bending load

a steady-state value is not reached, but this figure suggests that if the simulation were carried out for slightly lower strength, steady state would be reached. Recall that for this fiber strength matrix crack growth is accompanied by fiber failure. If a smaller fiber strength was used in the calculations the fiber bridging would be limited to a relatively small region behind the crack tip, and as the matrix crack propagates, for every fiber the crack crosses, a fiber behind the crack tip would fail. For $\sigma_{fu} = 3000$ MPa, the normalized applied stress intensity factor also increases monotonically. Although the simulations were not continued beyond $a/w = 0.8$, Fig. 16(c) suggests that the stress intensity factor would increase drastically as the matrix crack approaches the free edge.

Three-Point Bend Loading

The results presented in the preceding section demonstrate the effects initial crack length and fiber strength have on the stability of fiber failure. Similar results are presented next for the three-point bending case. These will demonstrate that the distribution of stresses that result from the applied loads also strongly influence the failure mechanisms.

Figures 17–20, which are similar to the figures presented for the constant tension loading, clearly show the effects of external loading on the stability of the bridged cracks. Figures 17–19 are for fixed a/w , while Fig. 20 is for a propagating

matrix crack. The load P is nondimensionalized with respect to the load P_0 , which represents the load that would produce a stress equal to σ_{fu} at the outer fibers in an unnotched monolithic beam made out of fiber material. Recall that for the constant tension specimen, the crack lengths $a/w = 0.02$ and 0.10 were stable, while cracks of length $a/w = 0.16$ and 0.2 exhibited instabilities in fiber failure. Moreover, the severity of the instabilities increased with increasing fiber strength. Figure 17(b) shows an instability in $a/w = 0.1$ at the lowest fiber strength. Furthermore, when the fiber failure stabilizes at point 8, 80 percent of the fibers behind the crack tip are broken. Figure 20 is the stress-displacement curve of a matrix crack propagating from an initially fully bridged length $a/w = 0.1$. The load increases to point 1, at which point the unbridged length is a $a_0/a = 0.8$ and the matrix crack propagates. If the stress is held constant there is a discontinuity in the curve and the matrix crack ends up at $a/w = 0.6$ at a relatively low stress.

The results clearly show that the bending specimen inherently more unstable than the constant tension specimen.

Conclusions and Recommendations

The examples considered in this paper clearly demonstrate that:

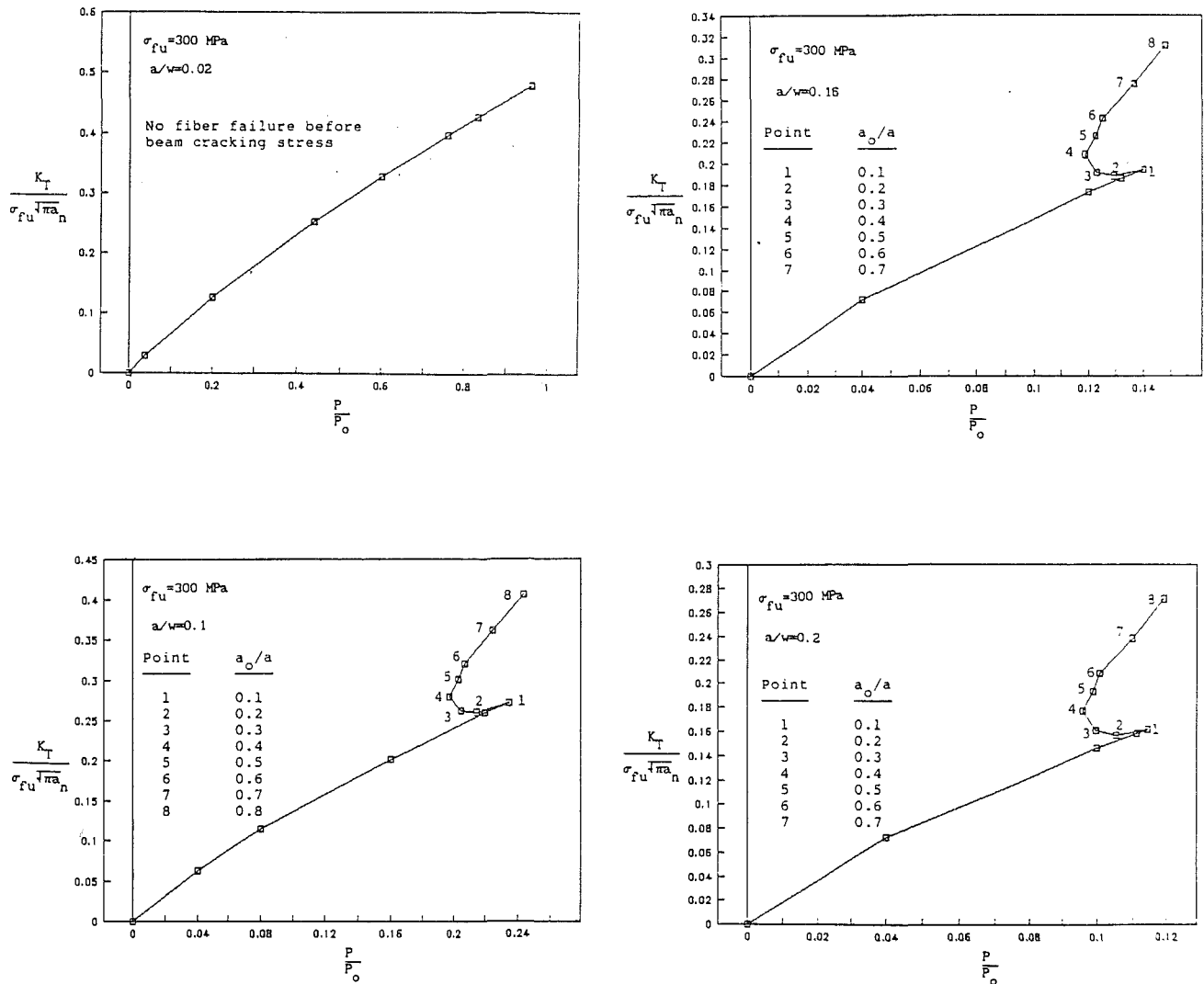


Fig. 18 Normalized stress intensity factor as functions of three-point bending load

1 Specimen configuration, distribution of applied loads, and constituent properties (fiber strength, etc.) *strongly* influence the amount of crack tip shielding the fibers provide in a bridged crack.

2 If two specimens having different configurations (or if they have the same configuration but are loaded differently) have the same *applied* stress intensity factor, their failure characteristics may differ significantly. One may fail catastrophically, while the other may fail noncatastrophically.

3 The critical stress for crack extension and the strain to failure for noncatastrophic failure are higher than for catastrophic failure.

4 As pointed out in [11], conclusions 1, 2, and 3 may lead to nonconservative predictions of material properties if current testing standards are applied to materials that exhibit crack bridging, since these procedures were developed for materials that do not exhibit crack bridging.

5 The bridging force-crack opening displacement (C.O.D.) relation $p(x) = p(\text{C.O.D.})$ should be included in analyses of experimental specimens or components. This relation should be treated as an engineering property of the material.

Acknowledgments

This work was funded by NASA Lewis Research Center

under Grant NAG3-856 and by the Defense Advanced Research Projects Agency through the University Initiative Program of C.W.R.U. under ONR Contract N-0013-86-K-0773. The first author thanks Dr. B. N. Cox for many helpful discussions and for providing us with unpublished manuscripts [10, 11].

References

- 1 Barenblatt, G. I., "The Mathematical Theory of Equilibrium Cracks in Brittle Fracture," *Advances in Appl. Mech.*, Vol. 7, 1962, pp. 55-129.
- 2 Dugdale, D. S., "Yielding of Steel Sheets Containing Slits," *J. Mech. Phys. Sol.*, Vol. 8, 1960, pp. 100-108.
- 3 Visalvanich, K., and Naaman, A. E., "Fracture Model for Fiber Reinforced Concrete," *ACI Journal*, Mar.-Apr. 1983, pp. 128-138.
- 4 Hillerborg, A., Modeer, M., and Petersson, P. E., "Analysis of Crack Formation and Crack Growth in Concrete by Means of Fracture Mechanics and Finite Elements," *Cement and Concrete Research*, Vol. 6, 1976, pp. 773-782.
- 5 Catalano, D. M., and Ingraffea, A. R., "Concrete Fracture: A Linear Elastic Fracture Mechanics Approach," Report No. 82-1, Department of Structural Engineering, Cornell University, 1982.
- 6 Ballarini, R., Shah, S. P., and Keer, L. M., "Crack Growth in Cement Based Composites: Influence of Fiber Strength," *Engineering Fracture Mechanics*, Vol. 20, 1984, pp. 433-445.
- 7 Marshall, D. B., Cox, B. N., and Evans, A. G., "The Mechanics of Matrix Cracking in Brittle-Matrix Fiber Composites," *Acta Metallurgica*, Vol. 33, 1985, pp. 2013-2021.
- 8 Marshall, D. B., and Cox, B. N., "Tensile Fracture of Brittle Matrix Composites," *Acta Metallurgica*, Vol. 35, 1987, pp. 2607-2619.

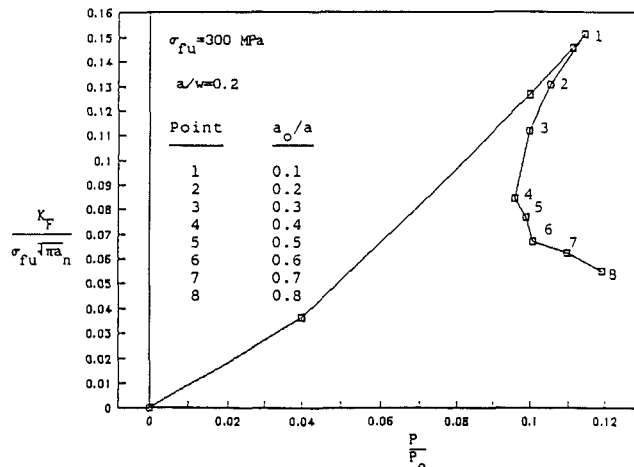
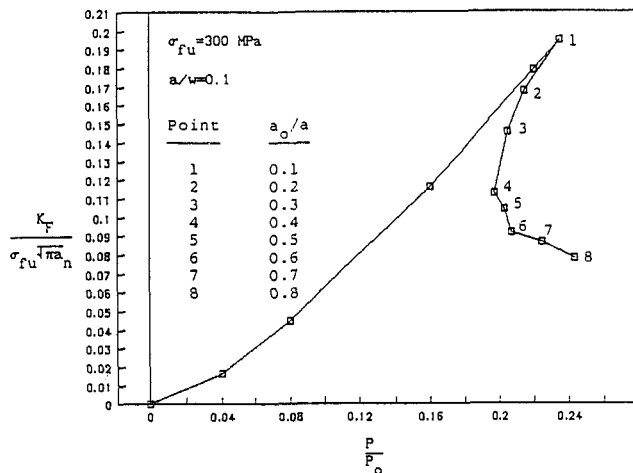
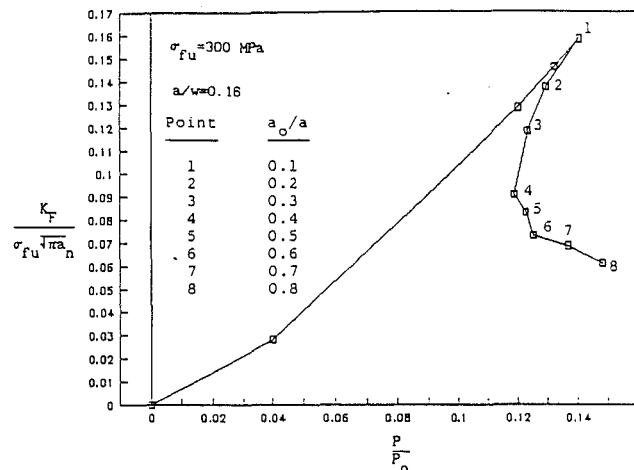
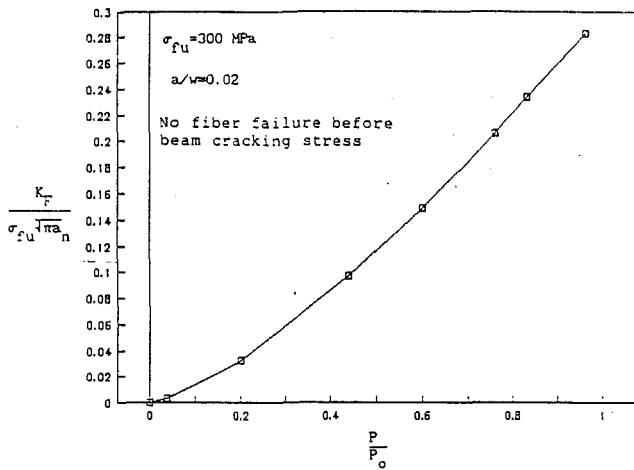


Fig. 19 Normalized shielding stress intensity factor as functions of three-point bending load

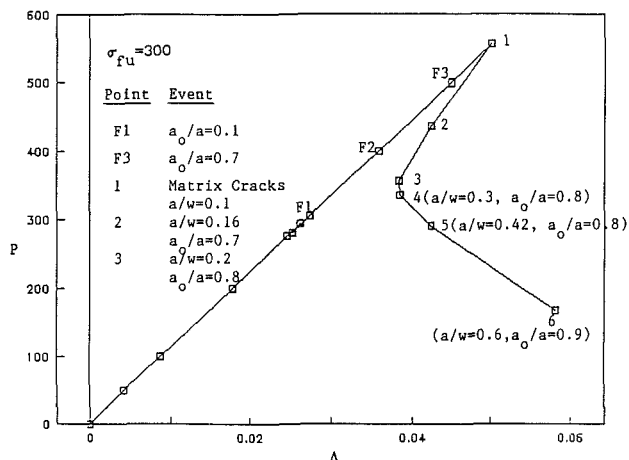


Fig. 20 Load-deflection curve for three-point bend specimen

9 Carpinteri, A., "Cusp Catastrophe Interpretation of Fracture Instability," *J. Mech. Phys. Sol.*, Vol. 37, 1989, pp. 567-582.

10 Cox, B. N., and Marshall, D. B., "Stable and Unstable Solutions for Bridged Cracks in Various Specimens," *Acta Metallurgica*, Vol. 39, 1991, pp. 579-589.

11 Cox, B. N., "Extrinsic Factors in the Mechanics of Bridged Cracks," submitted for publication.

12 Thouless, M. D., and Evans, A. G., "Effects of Pull-out on the Mechanical Properties of Ceramic-Matrix Composites," *Acta Metallurgica*, Vol. 36, 1988, pp. 517-522.

13 Muju, S., "Stability Analysis of Bridged Cracks in Ceramic Matrix Composites," M.S. Thesis, Case Western Reserve University, Jan. 1991.

14 Bowie, O. L., and Freese, C. E., "Central Crack in Plane Orthotropic Sheet," *International Journal of Fracture Mechanics*, Vol. 8, 1972, pp. 49-57.

15 More, J. J., Garbow, B. S., and Hillstrom, K. E., "User Guide for Minpack-1," Argonne National Lab ANL-80-74.

16 Ballarini, R., and Ahmed, S., "Local-Global Analysis of Crack Growth in Continuously Reinforced Ceramic Matrix Composites," *ASME JOURNAL OF ENGINEERING FOR GAS TURBINES AND POWER*, in press.

17 Kanninen, M. F., "Applications of Fracture Mechanics to Fiber Composite Materials and Adhesive Joints: A Review," *Proceedings of the 3rd International Conference on Numerical Methods in Fracture Mechanics*, Swansea, United Kingdom, 1984, pp. 641-680.